

₁ Study of neutrino-nucleus interaction at around 1 GeV using
₂ a 3D grid-structure neutrino detector, WAGASCI, muon
₃ range detectors and magnetized spectrometer, Baby MIND,
₄ at J-PARC neutrino monitor hall

₅ A. Bonnemaison, R. Cornat, L. Domine, O. Drapier, O. Ferreira, F. Gastaldi,
₆ M. Gonin, J. Imber, M. Licciardi, F. Magniette, T. Mueller, L. Vignoli, and O. Volcy
₇ *Ecole Polytechnique, IN2P3-CNRS, Laboratoire Leprince-Ringuet, Palaiseau,*
₈ *France*

₉ S. Cao and T. Kobayashi

₁₀ *High Energy Accelerator Research Organization (KEK), Tsukuba, Ibaraki, Japan*

₁₁ M. Khabibullin, A. Khotjantsev, A. Kostin, Y. Kudenko, A. Mefodiev, O. Mineev,
₁₂ S. Suvorov, and N. Yershov

₁₃ *Institute for Nuclear Research of the Russian Academy of Sciences, Moscow, Russia*

₁₄ B. Quilain

₁₅ *Kavli Institute for the Physics and Mathematics of the Universe (WPI), The*
₁₆ *University of Tokyo Institutes for Advanced Study, University of Tokyo, Kashiwa,*
₁₇ *Chiba, Japan*

₁₈ T. Hayashino, A. Hiramoto, A.K. Ichikawa, K. Nakamura, T. Nakaya, K Yasutome,
₁₉ and K. Yoshida

₂₀ *Kyoto University, Department of Physics, Kyoto, Japan*

₂₁ Y. Azuma, J. Harada, T. Inoue, K. Kin, N. Kukita, S. Tanaka, Y. Seiya,
₂₂ K. Wakamatsu, and K. Yamamoto

₂₃ *Osaka City University, Department of Physics, Osaka, Japan*

24 A. Blondel, F. Cadoux, Y. Favere, E. Noah, L. Nicola, and S. Parsa

25 *University of Geneva, Section de Physique, DPNC, Geneva, Switzerland*

26 N. Chikuma, F. Hosomi, T. Koga, R. Tamura, and M. Yokoyama

27 *University of Tokyo, Department of Physics, Tokyo, Japan*

28 Y. Hayato

29 *University of Tokyo, Institute for Cosmic Ray Research, Kamioka Observatory,
30 Kamioka, Japan*

31 Y. Asada, K. Matsushita, A. Minamino, K. Okamoto, and D. Yamaguchi

32 *Yokohama National University, Faculty of Engineering, Yokohama, Japan*

33 December 12, 2017

34 **1 Introduction**

35 The understanding of neutrino-nucleus interactions in the 1 GeV energy region is critical
36 for the success of accelerator-based neutrino oscillation experiments such as the T2K exper-
37 iment. Complicated multi-body effects of nuclei render this understanding difficult. The
38 T2K near detectors have been measuring these and significant progress has been achieved.
39 However, the understanding is still limited. One of the big factors preventing from full
40 understanding is the non-monochromatic neutrino beam spectrum. Measurements with
41 different but some overlapping beam spectra would greatly benefit to resolve the contri-
42 bution from different neutrino energies. We, the Wagasci collaboration, proposes to study
43 the neutrino-nucleus interaction at the B2 floor of the neutrino monitor building, where
44 different neutrino spectra can be obtained due to the different off-axis position. Our exper-
45 imental setup contains 3D grid-structure plastic-scintillator detectors filled with water as
46 the neutrino interaction target (Wagasci modules), two side- and one downstream- muon
47 range detectors(MRD's). The 3D grid-structure and side-MRD's allows a measurement of
48 wider-angle scattering than the T2K off-axis near detector (ND280). High water to scintil-
49 lator material ratio enables the measurement of the neutrino interaction on water, which
50 is highly desired for the T2K experiment because it's far detector, Super-Kamiokande,

51 is composed of water. The MRD's consist of plastic scintillators and iron plates. The
52 downstream-MRD, so called the Baby MIND detector, also works as a magnet and pro-
53 vides the charge identification capability as well as magnetic momentum measurement for
54 high energy muons. The charge identification is essentially important to select antineu-
55 trino events in the antineutrino beam because contamination of the neutrino events is as
56 high as 30%. Most of the detectors has been already constructed. The Wagasci modules
57 have been commissioned as the J-PARC T59 experiment and the Baby MIND detector was
58 commissioned at the CERN neutrino platform. Therefore, the collaboration will be ready
59 to proceed to the physics data taking for the T2K beam time in January 2019. We will
60 provide the cross sections of the charged current neutrino and antineutrino interactions on
61 water with slightly higher neutrino energy than T2K ND280 with wide angler acceptance.
62 When combined with ND280 measurements, our measurement would greatly improve the
63 understanding of the neutrino interaction at around 1 GeV and contribute to reduce one
64 of the most significant uncertainty of the T2K experiment.

65 **2 Experimental Setup**

66 Figure. 1 shows a schematic view of the entire set of detectors. Central neutrino target
67 detectors consist of two Wagasci modules and T2K INGRID proton module. Inside the
68 Wagasci module, plastic scintillator bars are aligned as a 3D grid-like structure and spaces
69 in the structure are filled with water for a water-in Wagasci module. T2K INGRID proton
70 module is a full active neutrino target detector which is composed only with scintillator
71 bars in its tracking region. The central detectors are surrounded by two side- and one
72 downstream- muon range detectors(MRD's) The MRD's are used to select muon tracks
73 from the charged-current (CC) interactions and to reject short tracks caused by neutral
74 particles that originate mainly from neutrino interactions in material surrounding the cen-
75 tral detector, like the walls of the detector hall, neutrons and gammas, or neutral-current
76 (NC) interactions. The muon momentum can be reconstructed from its range inside the
77 detector. The MRD's consist of plastic scintillators and iron plates. In addition, each of
78 the iron plates of the downstream-MRD, so called the Baby MIND detector, is wound by
79 a coil and can be magnetized. It provide the charge selection capability.

80 For all detectors, scintillation light in the scintillator bar is collected and transported
81 to a photodetector with a wavelength shifting fiber (WLS fiber). The light is read out by
82 a photodetector, Multi-Pixel Photon Counter (MPPC), attached to one end of the WLS
83 fiber. The signal from the MPPC is read out by the dedicated electronics developed for the
84 test experiment to enable bunch separation in the beam spill. The readout electronics is
85 triggered using the beam-timing signal from MR to synchronize to the beam. The beam-
86 timing signal is branched from those for T2K, and will not cause any effect on the T2K
87 data taking.

88 T2K adopted the off-axis beam method, in which the neutrino beam is intentionally

tmp.pdf

Figure 1: Schematic view of entire sets of detectors.

89 directed 2.5 degrees away from SK producing a narrow band ν_μ beam. The off-axis near
90 detector, ND280, is installed towards the SK direction in the B1 floor of the near detector
91 hall of the J-PARC neutrino beam-line. We propose to install our detector in the B2 floor
92 of the near detector hall, where the off-axis angle is similar but slightly different: 1.5 degree.
93 The candidate detector position in the B2 floor is shown in Fig. 2. The expected neutrino
94 energy spectrum at the candidate position is shown in Fig. 3.

95 **2.1 Wagasci module**

96 The dimension of the each Wagasci module is 100cm \times 100cm in the x and y directions
97 and 50cm along the beam direction. Inside the Wagasci module, plastic scintillator bars
98 are aligned as a 3D grid-like structure, shown in Fig. 7, and spaces in the structure are
99 filled with water for the water-in Wagasci module.

100 The total water mass serving as neutrino targets are \sim 0.5 ton. When neutrinos interact
101 with hydrogen, oxygen or carbon, in water and scintillators, charged particles are generated.
102 Neutrino interactions are identified by detecting tracks of charged particles through plastic
103 scintillation bars. Thanks to the 3 D grid-like structure of the scintillator bars, the Wagasci
104 module has 4π angular acceptance for charged particles. Furthermore, adopting a 5cm grid
105 spacing, short tracks originated from protons and charged pions can be reconstructed with
106 high efficiency. Thin plastic scintillator bars (thickness \sim 0.3cm) are used for the Wagasci
107 module to reduce the mass ratio of scintillator bars to water, because neutrino interactions
108 in the scintillator bars are a background for the cross section measurements. Scintillator
109 bars whose dimensions are 2.5cm x 0.3cm x 100cm are used for the Wagasci module. The

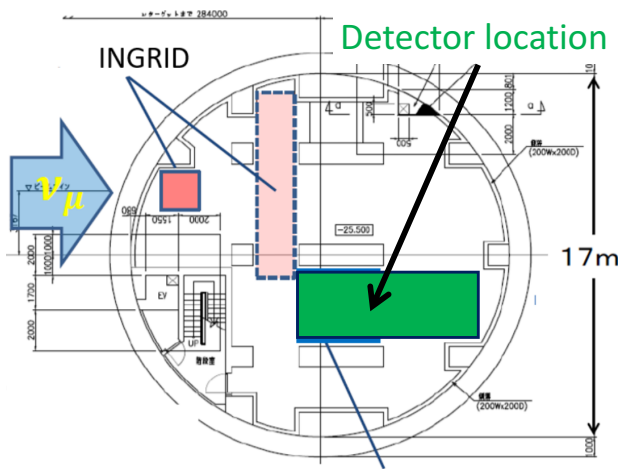


Figure 2: Candidate detector position in the B2 floor of the near detector hall.

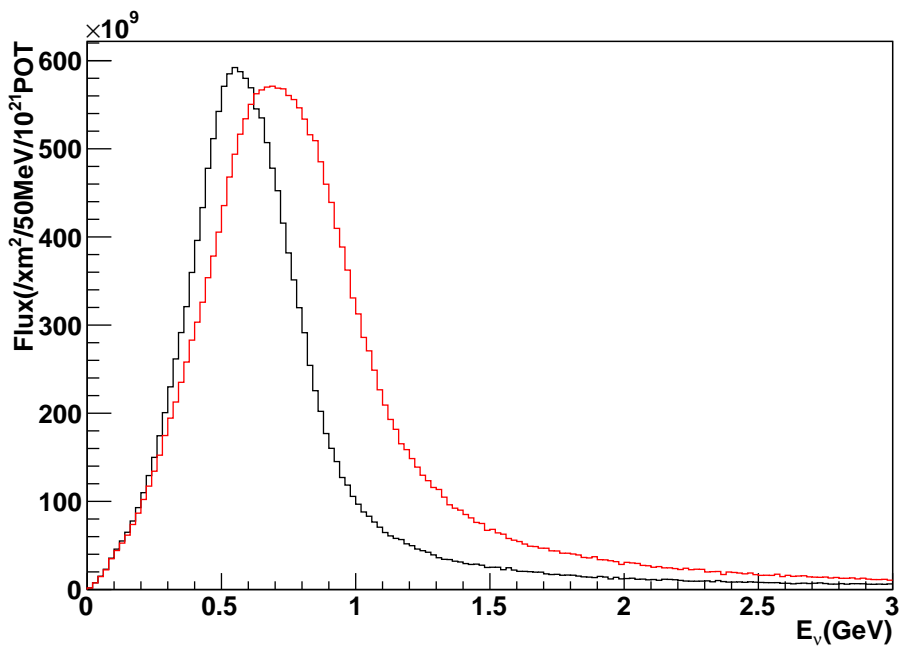


Figure 3: Neutrino energy spectrum at the candidate detector position (red, off-axis 1.5 degree). The spectrum at the ND280 site (black, off-axis 2.5 degree) is also shown.

110 total number of channels in one Wagasci module is 1280.

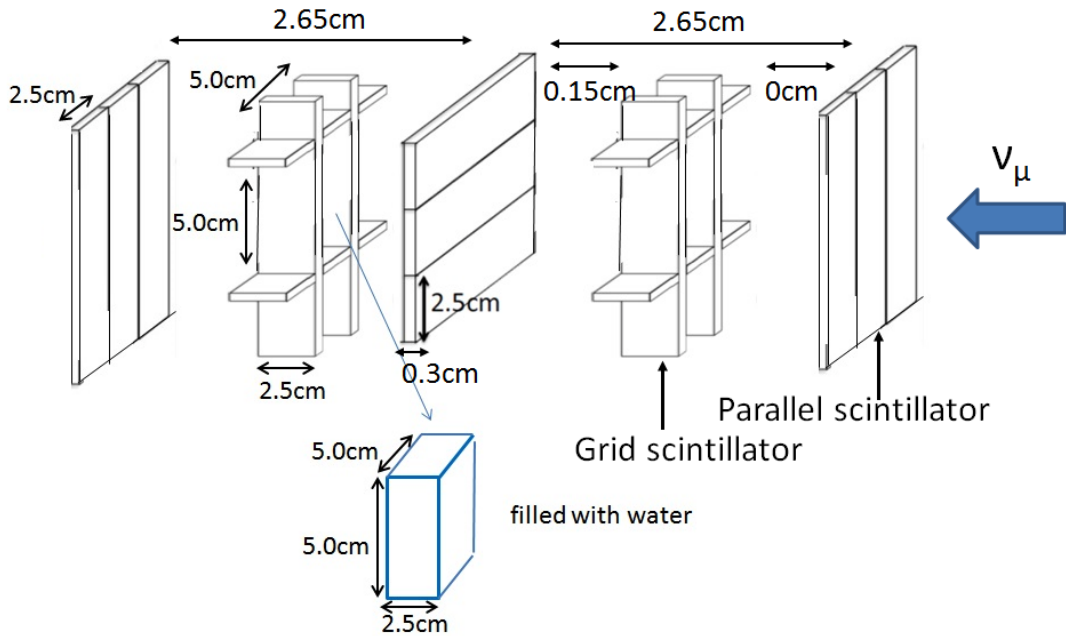


Figure 4: Schematic view of 3D grid-like structure of plastic scintillator bars inside the central detector.

111 2.2 INGRID Proton module

112 INGRID Proton module is a neutrino detectors of the T2K experiment. It is composed only
113 with scintillator bars in its tracking region. (Add more explanation here.) It was installed
114 at the neutrino beam axis on the SS floor of the T2K near detector hall in 2010, and had
115 been used for neutrino cross section measurements. In August 2017, it was moved to the
116 B2 floor of the same detector hall by J-PARC T59 after getting the approval from T2K
117 to use them. J-PARC T59 is performing neutrino beam measurement using the detector
118 from October 2017, and the measurement will continue until May 2018.

119 2.3 Baby MIND

120 The Baby MIND is the downstream Muon Range Detector. It also works as a magnet and
121 provides the charge identification capability as well as magnetic momentum measurement
122 for high energy muons.

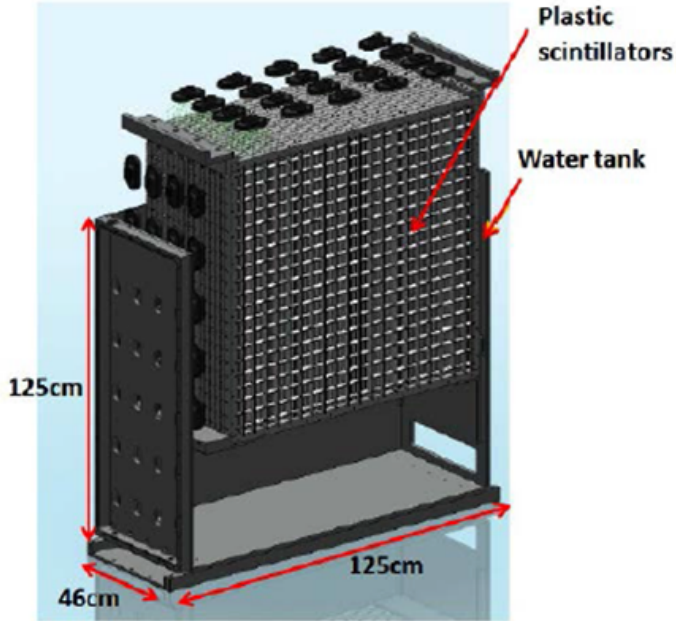


Figure 5: Schematic view of Wagasci module.

123 The Baby MIND collaboration ¹ submitted a proposal to the SPSC at CERN, SPSC-P-
 124 353. The project was approved by the CERN research board as Neutrino Platform project
 125 NP05 and constructed. The detector consists of 33 magnet modules, each 3500 mm ×
 126 2000 mm × 50 mm (30 mm steel) with a mass of approximately 2 tonnes. Of these magnet
 127 modules, 18 are instrumented with plastic scintillator modules.

128 2.3.1 Magnet modules

129 The Baby MIND is built from sheets of iron interleaved with scintillator detector modules
 130 but unlike traditional layouts for magnetized iron neutrino detectors (e.g. MINOS) which
 131 tend to be monolithic blocks with a unique pitch between consecutive steel segments and
 132 large conductor coils threaded around the whole magnet volume, the Baby MIND iron seg-
 133 ments are all individually magnetized as shown in Fig. 8, allowing for far greater flexibility
 134 in the setting of the pitch between segments, and in the allowable geometries that these
 135 detectors can take.

136 The key design outcome is a highly optimized magnetic field map. A double-slit con-
 137 figuration for coil winding was adopted to increase the area over which the magnetic flux

¹Contact person: E. Noah, Spokesperson: A. Blondel, Deputy spokesperson: Y. Kudenko

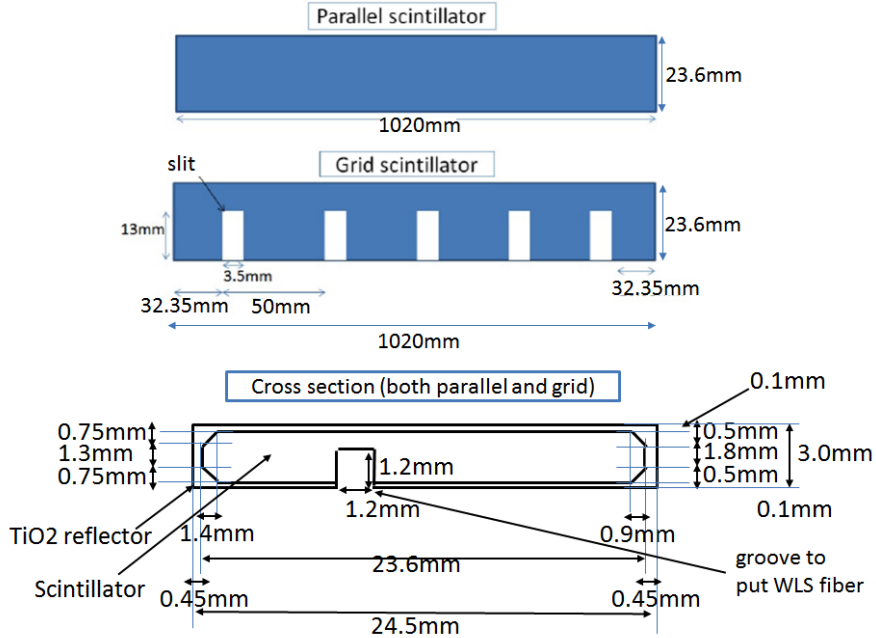


Figure 6: Geometry of scintillators used for Wagasci modules.

138 lines are homogeneous in B_x across the central tracking region. Simulations show the
 139 magnet field map to be very uniform over this central tracking region covering an area of
 140 $2800 \times 2000 \text{ mm}^2$, Fig. 9. The B_x component dominates in this region, with negligible B_y
 141 and B_z . This was confirmed by measuring the field with 9 pick-up coils wound around the
 142 first module. Subsequent modules were equipped with one pick-up coil. Test results on
 143 the 33 modules show all to achieve the required field of 1.5 T for a current of 140 A, with
 144 a total power consumption of 11.5 kW. The polarity of the field map shown in Figure 9
 145 (middle) can be reversed by changing the power supply configuration.

146 **2.3.2 Scintillator modules**

147 Each of the 18 scintillator modules is constructed from 2 planes of horizontal counters (95
 148 counters in total) and 2 planes of vertical counters (16 counters in total) [?], arranged
 149 with an overlap between planes to achieve close to 100% hit efficiency for minimum ionizing
 150 muons. The arrangement of planes within a module is vertical-horizontal-horizontal-
 151 vertical. This arrangement was the result of an assembly approach whereby each plane
 152 was built from 2 half-planes, with each half plane consisting of a horizontal plane and a
 153 vertical plane. The scintillator bars are held in place using structural ladders that align
 154 and maintain the counters, Figure 10. No glue is used in the process, so counters can be

tmp.pdf

Figure 7: tmp.

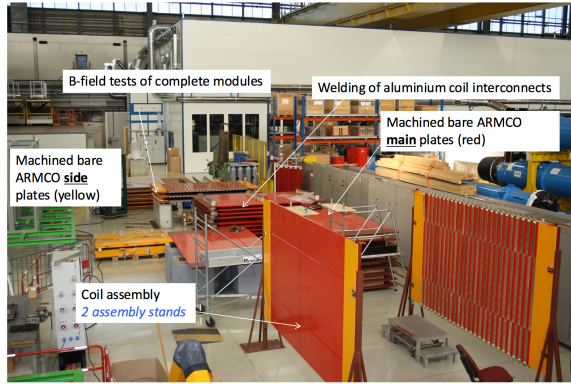


Figure 8: Magnet assembly zone at CERN.

155 replaced. Aluminum sheets front and back provide light tightness.

156 The plastic scintillator counters were made from 220 mm-wide slabs, consisting of
157 extruded polystyrene doped with 1.5% paraterphenyl (PTP) and 0.01% POPOP. They were
158 cut to size then covered with a 30-100 μm thick diffuse reflector resulting from etching of
159 the surface with a chemical agent [?, ?]. The horizontal counter size is $2880 \times 31 \times 7.5 \text{ mm}^3$,
160 with one groove along the length of the bar in which sits a wavelength shifting fiber from
161 Kuraray. The vertical counter size is $1950 \times 210 \times 7.5 \text{ mm}^3$, with one U-shaped groove
162 along the bar. On each counter, two custom connectors house silicon photomultipliers,
163 MPPC type S12571-025C from Hamamatsu, either side of the horizontal counter, and
164 both connectors at the top for the vertical counter. This geometrical configuration for
165 vertical counters was chosen for ease of connectivity to the electronics, and maintenance
166 operations.

167 A total of 1744 horizontal counters and 315 vertical counters (including spares) were

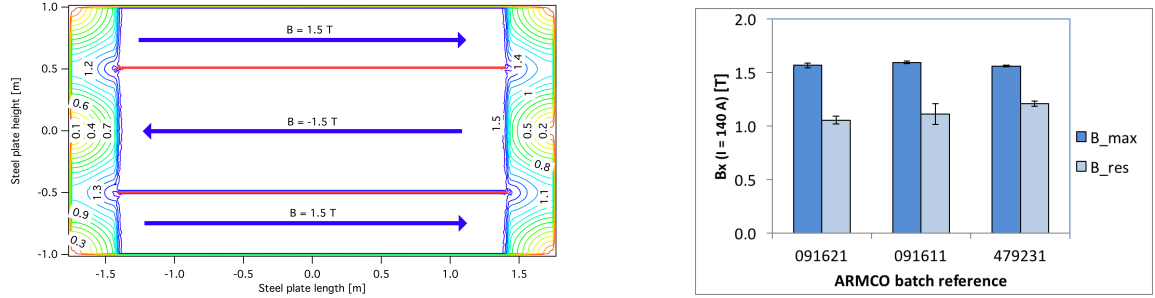


Figure 9: Left) Magnetic field map with a coil along 280 cm of the length of the plate. Right) Measured B field for 33 modules.



Figure 10: Scintillator modules assembly. Left) top of front half-module showing vertical counters, and the spacers-ladders that set the pitch between horizontal counters and hold them in place. Middle) rear half-module showing horizontal counters on their ladders. Right) Assembled rear half-module, the front half-module can be seen in the background.

¹⁶⁸ produced at the Uniplast company (Vladimir, Russia).

¹⁶⁹ 2.3.3 Electronics

¹⁷⁰ The Baby MIND electronic readout scheme includes several custom-designed boards ^[?].
¹⁷¹ The revised version is shown in Figure 11. At the heart of the system is the electronics
¹⁷² Front End Board (FEB), developed by the University of Geneva. The readout system
¹⁷³ includes two ancillary boards, the Backplane, and the Master Clock Board (MCB) whose
¹⁷⁴ development has been managed by INRNE (Bulgarian Academy of Sciences) collaborators.

¹⁷⁵ The FEBv2 hosts 3 CITIROC chips that can each read in signals from 32 SiPMs ^[?].
¹⁷⁶ Each signal input is processed by a high gain, and a separate low gain, signal path. The
¹⁷⁷ outputs from the slow shapers can be sampled using one of two modes: a mode with an
¹⁷⁸ externally applied delay, and a peak detector mode. A faster shaper can be switched to
¹⁷⁹ either HG or LG paths, followed by discriminators with adjustable thresholds providing 32
¹⁸⁰ individual trigger outputs and one OR32 trigger output. An Altera ARIA5 FPGA on the
¹⁸¹ FEBv2 samples these trigger outputs at 400 MHz, recording rising and falling times for

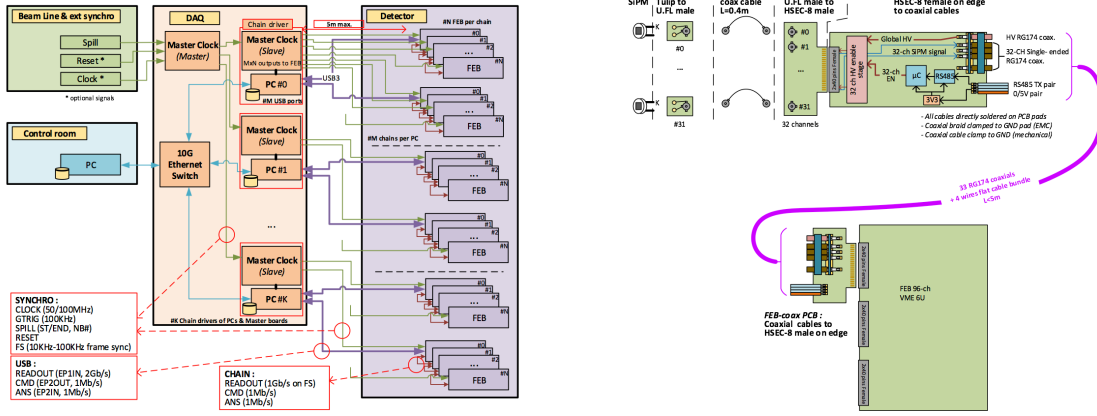


Figure 11: Left) Baby MIND electronics readout scheme. Right) SiPM-to-FEB connectivity.

the individual triggers and assigning time stamps to these. Time-over-threshold from the difference between falling and rising times gives some measure of signal amplitude, used in addition to charge information and useful if there is more than one hit per bar within the deadtime due to the readout of the multiplexed charge output of $\sim 9 \mu\text{s}$. The ARIA5 also manages the digitization of the sampled CITIROC multiplexed HG and LG outputs via a 12-bit 8-ch ADC.

The internal 400 MHz clock on the FEBv2 can be synchronized to a common 100 MHz clock. The synchronization subsystem combines input signals from the beam line into a digital synchronization signal (SYNC) and produces a common detector clock (CLK) which can eventually be synchronised to an external experiment clock. Both SYNC and CLK signals are distributed to the FEBs. Tests show the FEB-to-FEB CLK(SYNC) delay difference to be 50 ps (70 ps). Signals from the beam line at WAGASCI include two separate timing signals, arriving 100 ms and 30 μs before the neutrino beam at the near detectors. The spill number is available as a 16-bit signal.

2.4 Side muon range detector

Four Side-MRD modules for tracking secondary particles from neutrino interactions will be constructed by the end of January 2018. Each Side-MRD module is composed of 11 steel plates and 10 layers of total 80 scintillator slabs installed in 13 mm gaps between the 30 mm thick plates. Each steel plate size is $30 \times 1610 \times 1800 \text{ mm}^3$. Total module size is $2236 \times 1630 \times 975 \text{ mm}^3$ as shown in Fig. 12, weight is ~ 8.5 ton.

Scintillator bars were manufactured by Uniplast company in Vladimir, Russia. Polystyrene based scintillators were extruded with thickness of 7 mm, then cut to the size of $7 \times 200 \times 1800 \text{ mm}^3$. Dopant composition is 1.5% PTP and 0.01% POPOP. Scintillator surface was

205 etched by a chemical agent to form a white diffuse layer with excellent reflective performance.
 206 Ideal contact between the scintillator and the reflector raises the light yield up to
 207 50% comparing to an uncovered scintillator. Sine like groove was milled along the scin-
 208 tillator to provide uniform light collection over the whole scintillator surface. WLS Y11
 209 Kuraray fiber of 1 mm diameter is glued with an optical cement EJ-500 in the S-shape
 210 groove as shown in Fig. 13. Bending radius is fixed to 30 mm that was specified to be safe
 211 for Kuraray S-type fibers. Both ends of the fiber are glued into optical connectors (Fig.
 212 14) which mounted within a scintillator body.

213 The plastic molded connectors provide an interface to SiPMs, Hamamatsu MPPC
 214 S13081-050CS(X1) used for the WAGASCI detector. Optical coupler of this type (so-called
 215 Baby-mind type of optical connector) consists of two parts (see Fig. 14): an container for
 216 the MPPC and a ferrule with the fiber. The ferrule is glued in the scitillator, and its end
 217 with glued in WLS fiber was polished. Both parts of the optical coupler are latched by a
 218 snap-like mechanism: a locking groove inside the container and matching ring protuber-
 219 ance on the ferrule. To ensure the optical contact a foam spring made of sponge rubber
 220 presses the MPPC to the fiber end (Fig. 15).

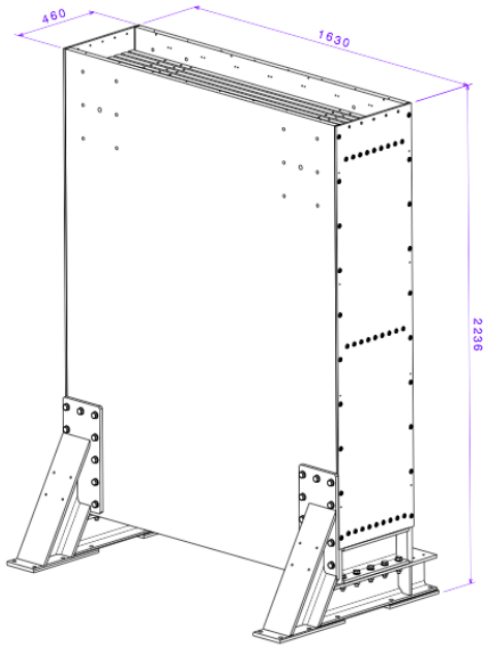


Figure 12: Support structure of the Side-MRD module.

221 Scintillators for the Side-MRD modules had been assembled at INR in Russia, and
 222 shipped to Japan in July 2017. The light yield for each scintillator was measured with

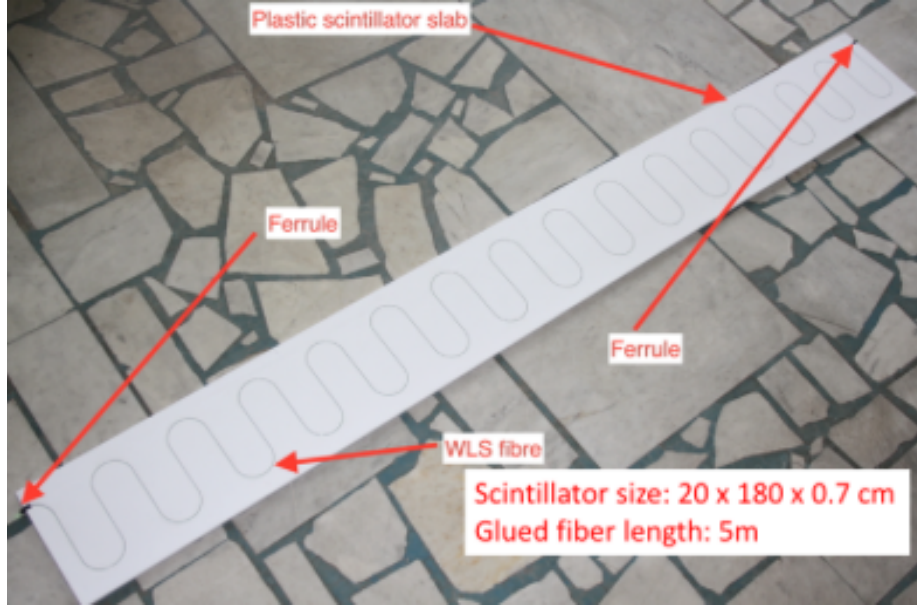


Figure 13: Scintillator bar of the Side-MRD modules.

223 cosmic rays at INR and at YNU in Japan after delivery. Parameters measured at the
 224 center of the counter were : the light yields LY_1 and LY_2 at both ends, the light yield
 225 asymmetry between the ends calculated as $100\% \times \frac{LY_1 - LY_2}{LY_1 + LY_2}$. After tests at INR we selected
 226 324 counters from measured 332 ones with the mean light yield of 45 p.e./MIP ($LY_1 + LY_2$
 227) and the asymmetry value less than 10 %. The measuremens at YNU yielded the average
 228 total light yield of about 40 p.e./MIP which varies in range from 32 to 50 p.e./MIP (Fig.
 229 16 (left)). Only two counters showed relatively high asymmetry close to 25 % as shown in
 230 Fig. 16 (right). Using the results of the quality assurance test we selected 320 scintillator
 231 counters for the Side-MRD modules.

232 We also measured the time resolution for a combination of four counters piled each on
 233 another one. Time resolution for a single counter is determined as rms of $(T_{left} - T_{right})/2$
 234 distribution. The difference of times was chosen to remove the correlated time fluctuation
 235 caused by a start trigger signal. The average result for four counters is $\sigma_T = 1.04$ ns
 236 (Upper left plot in Fig. 17). For a set of n counters the time resolution is calculated as
 237 $\frac{(T_L - T_R)_1 + (T_L - T_R)_2 + \dots + (T_L - T_R)_n}{2 \times n}$. The result of combination of 2, 3, 4 counters is 0.79 ns,
 238 0.66 ns and 0.58 ns, correspondently (Fig. 17).

239 Construction of Side-MRD modules will be done from November 2017 to January 2018

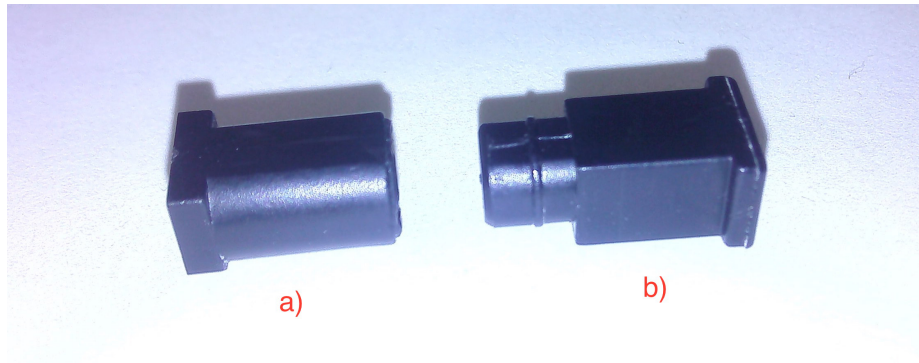


Figure 14: Optical connector for the Side-MRD scintillator. a) MPPC cover. b) Ferrule.

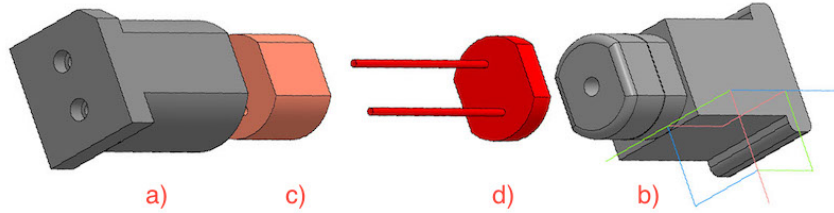


Figure 15: Scheme of the MPPC placement in optical connector. a) MPPC cover. b) Ferrule. c) Spring (sponge rubber). d) MPPC.

²⁴⁰ at Yokohama National University, then they will be transported to J-PARC and will be
²⁴¹ installed at B2 floor of the T2K near detector hall before T2K beam in March 2018.

²⁴² 3 Physics goals

²⁴³ We will measure the differential cross section for the charged current interaction on H₂O
²⁴⁴ and Hydrocarbon(CH)). The water-scintillator mass ratio of the Wagasci module is as
²⁴⁵ high as 5:1 and the high purity measurement of the cross section on H₂O is possible. One
²⁴⁶ experimental option is to remove water from one of the two Wagasci modules. The water-
²⁴⁷ out WAGASCI module will allow to measure pure-CH target interactions with very low
²⁴⁸ momentum-threshold for protons. It will also benefit to subtract the background from
²⁴⁹ interaction with scintillator in the water target measurement. Another option is to add
²⁵⁰ the T2K proton module which is fully made of plastic scintillators. It will allow the high
²⁵¹ statistics comparison of cross section between H₂O and CH and also comparison with

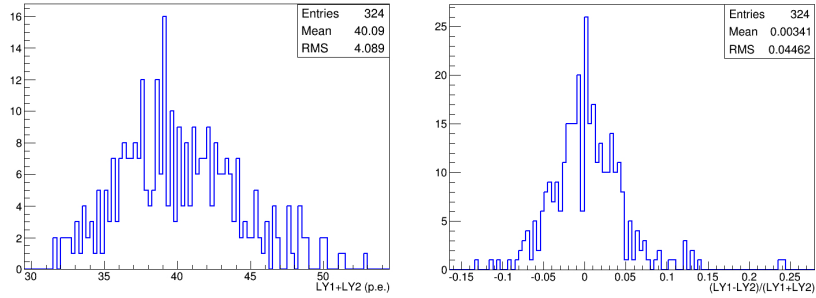


Figure 16: Total light yield distribution (left) and light yield assymetry (right) measured at YNU.

252 the ND280 measurement. The actual configuration will be optimized with detailed MC
253 simulation by 2018 Summer.

254 Our setup allows the measurements of inclusive and also exclusive channels such as $1-\mu$,
255 $1-\mu 1p$, $1-\mu 1\pi \pm np$ samples, former two of which are mainly caused by the quasi-elastic and
256 2p2h interaction and the latter is mainly caused by resonant or coherent pion production
257 and deep elastic scattering. In general, an accelerator produced neutrino beam spectrum
258 is wide and the energy reconstruction somehow rely on the neutrino interaction model.
259 Therefore, recent neutrino cross section measurement results including those from T2K
260 are given as a flux-integrated cross section rather than cross sections as a function of
261 the neutrino energy to avoid the model dependency. We can provide the flux-averaged
262 cross section. In addition, by combining our measurements with those at ND280, model-
263 independent extraction of the cross section for narrow energy region becomes possible.
264 This method was demonstrated in [?] and also proposed by P** (NUPRISM).

265 3.1 Expected number of events

266 Expected number of neutrino events after the event selections is evaluated with Monte
267 Carlo simulations as we will discuss in Section 6. 2.41×10^4 CC events are expected in
268 two WAGASCI modules after the selection with 1×10^{20} POT in neutrino-mode, and its
269 purity is 75.5 %. In case we choose the option with one WAGASCI module and the T2K
270 proton module, 1.2×10^4 CC events are expected in the WAGASCI module and $\sim 1 \times 10^4$
271 CC events are expected in the T2K proton module. In case we choose the option with one
272 water-in WAGASCI module and one water-out WAGASCI module, 1.2×10^4 CC events are
273 expected in the water-in module and 0.24×10^4 CC events are expected in the water-out
274 module.

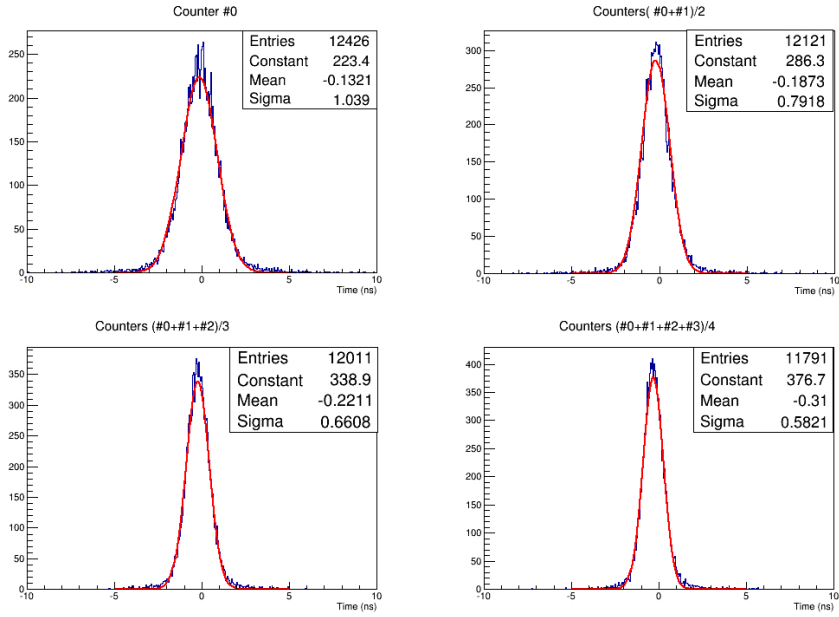


Figure 17: Time resolution for one (upper left) and a set of 2,3,4 Side-MRD counters.

275 3.2 Pseudo-monochromatic beam by using different off-axis fluxes

276 The off-axis method gives narrower neutrino spectrum, and the peak energy is lower for
 277 larger off-axis angle. There still remains high energy tail mainly due to neutrinos from
 278 Kaon decay. The off-axis angle of the Wagasci location is 1.5 degree and different from the
 279 ND280 2.5 degree. Top two plots of Fig. 18 show the energy spectra of fluxes and neutrino
 280 interaction events at these two different location. The high energy tail of ND280 flux can
 281 be somehow subtraction by using the Wagasci measurement. The low energy part of the
 282 Wagasci flux can be also subtracted by using the ND280 measurement. Bottom two plots
 283 of Fig. 18 demonstrate this method. We can effectively get two fluxes, from 0.2 GeV to
 284 0.9 GeV and 0.6 GeV and 2 GeV and measure flux-integrated cross section for these two
 285 fluxes.

286 3.3 Subjects Wagasci can contribute

287 In T2K experiment, neutrinos interact with bound nucleons in relatively heavy nuclei
 288 (Carbon and Oxygen), so the cross-section is largely affected by nuclear effects. The nuclear
 289 effects are categorized as nucleons' momentum distribution in nucleus, interactions with
 290 correlated pairs of nucleons in nucleus (two particles-two holes, 2p2h), collective nuclear
 291 effects calculated with Random Phase Approximation (RPA) and final state interactions

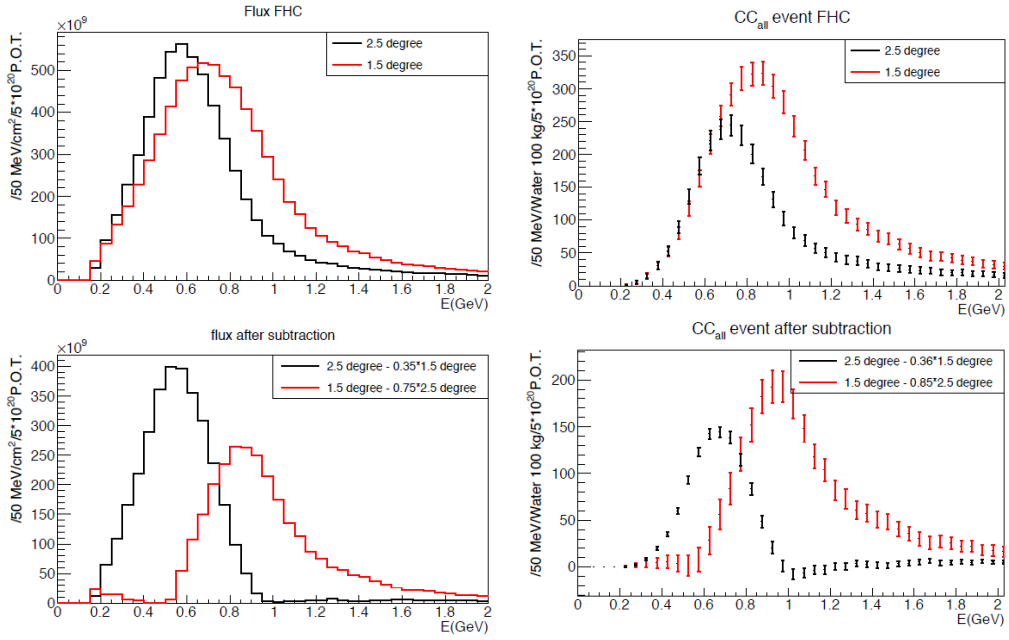


Figure 18: Energy spectra obtained by using different off-axis angle fluxes. Top two plots show the fluxes(left) and spectra of interaction events (right) for ND280 (off-axis 2.5 degree) and Wagasci (off-axis 1.5 degree). Bottom two plots show the fluxes (left) and spectra of interaction events (right) obtained by subtraction of fluxes at ND280 and Wagasci. The error bar is for the statistical error and those in the bottom right plot is obtained assuming the statistical error for ND280 measurement is much smaller than that of Wagasci experiment.

(FSI) of secondary particles in the nuclei after the initial neutrino interactions.

The 2p2h interactions mainly happen through Δ resonance interactions following a pion-less decay and interactions with a correlated nucleon pair. The 2p2h interactions are observed in electron scattering experiments (add ref. here) where the 2p2h events observed in the gap between Quasi-Elastic region and Pion-production region as shown in Fig. ???. Neutrino experiments also attempt to measure the 2p2h interactions, but separation of the QE peak and the 2p2h peak is more difficult because transferred momentum (p) and energy (w) are largely affected by neutrino energies which cannot be determined event-by-event in the wide energy spectrum of the accelerator neutrino beam. Our model-independent narrow neutrino spectra extracted from combined analyses of our data and ND280 data are ideal for searching the 2p2h interaction because clearer separation of the QE peak and the 2p2h peak is expected. Another way to observe the 2p2h interaction is direct measurement of proton tracks in CC 0π sample with low detection threshold and full acceptance. Fig. ??

305 shows proton multiplicities in CCQE events and 2p2h events, and Fig. ?? shows opening
306 angles among two proton tracks in the same samples. The water-out WAGASCI can provide
307 good sample for the 2p2h interaction search because its low density medium enables the
308 detection of low momentum protons in addition to the full acceptance.

309 The corrections from collective nuclear effects calculated by RPA as a function of Q^2 are
310 shown in Fig. ???. The Q^2 dependence of the correction can be tested by measuring angular
311 distribution of muons in CC1- μ and CC1- $\mu 1p$ events. The uncertainties of the corrections
312 in low (high) Q^2 regions can be constrained by observing the events with a forward-going
313 (high-angle) muon, so it is essential to measure muon tracks with full acceptance.

314 T2K experiment is starting to use ν_e CC1 π events for its CP violation search to increase
315 the statistics. One of the biggest uncertainty of the CC1 π sample comes from the final
316 state interactions of pions in the nuclei after the initial neutrino interactions because they
317 change the multiplicity, charge and kinematics of the pions. The multi-pion production
318 events can be migrated into the CC1 π sample due to the FSIs, and they become important
319 backgrounds. We can constrain the uncertainties from the pion FSIs by measuring pion
320 rescattering in the detector and pion multiplicity in ν_μ CCn π sample with low detection
321 threshold and full acceptance for pion tracks. The water-out WAGASCI can provide good
322 sample for the pion FSI studies because its low density medium enables the detection of
323 low momentum pions in addition to the full acceptance.

324 4 Status of J-PARC T59 experiment

325 We had submitted a proposal of a test experiment to test a new detector with a water
326 target, WAGASCI, at the T2K near detector hall to J-PARC PAC on April 2014, and the
327 proposal was approved as J-PARC T59. There are several updates on the project after
328 three years from then. Fist, the start time of neutrino beam measurement is changed from
329 December 2015 to October 2017, and the requested neutrino beam is changed from 1×10^{21}
330 POT of ν beam to 0.8×10^{21} POT of anti- ν beam. Second, the detector configuration is
331 changed. In the original proposal, central neutrino detector are expected to be surrounded
332 by newly developed muon-range detectors (MRDs), but we will use spare neutrino detectors
333 of the T2K experiment instead of them during neutrino beam measurement from October
334 to December 2017. Construction of the newly developed MRDs, Baby-MIND and Side-
335 MRD, is in progress, and they will be installed to the both sides and the downstream of
336 the central neutrino detector from January to March 2018. Then, we will resume neutrino
337 beam measurements from March 2018 and will take the neutrino beam data until May
338 2018.

339 4.1 On-axis beam measurement with Prototype detector

340 Add INGRID water module measurement here.

341 **4.2 Plans from October 2017 to May 2018**

342 J-PARC MR will extract its proton beam to T2K neutrino beam-line from October to
343 December 2017, and, from March to May 2018. T2K experiment will produce anti-neutrino
344 beam and will accumulate $\sim 8 \times 10^{20}$ POT data during the above period.

345 J-PARC T59 will perform neutrino beam measurements on the B2 floor of the T2K
346 near neutrino detector hall during the above period to test basic performances of the
347 WAGASCI detector and new electronics. During the beam measurements from October to
348 December 2017, one WAGASCI module will be placed between spare neutrino detectors of
349 the T2K experiment, INGRID Proton module and INGRID standard module. Here, the
350 INGRID Proton module is used as a charged particle VETO detector and, the INGRID
351 standard module is used as a downstream muon detector. We had submitted a proposal
352 to use these spare neutrino detectors for the T59 neutrino beam measurements to the T2K
353 collaboration, and we got an approval from T2K.

354 During the beam measurements from March to May 2018, Baby-MIND and two side
355 muon-range detector (Side-MRD) modules will be installed on the downstream and the
356 both sides of the WAGASCI detector, as shown in Fig. 19, to increase angular acceptance
357 for secondary charged particles from neutrino interactions. Add Baby-MIND commissioning
358 items here!!!

tmp.pdf

Figure 19: J-PARC T59 detector configuration with Baby-MIND and two Side-MRD modules from Mar. to May 2018. (Need to prepare the figure.)

359 Expected number of neutrino events in the WAGASCI detector during the above beam
360 period is evaluated with Monte Carlo simulations. Neutrino beam flux at the detector
361 location is simulated by T2K neutrino flux generator, JNUBEAM, neutrino interactions

362 with target materials are simulated by a neutrino interaction simulator, NEUT, detector
363 responses are simulated using GEANT4-based simulation. The neutrino flux at the detector
364 location, 1.5 degrees away from the J-PARC neutrino beam axis, is shown in Figure 3, and
365 its mean neutrino energy is around 0.68 GeV. An event display of the GEANT4-based
366 detector simulation is shown in Figure 22.

367 To perform the detector performance test, the following event selections are applied to
368 the data. First, track reconstructions are performed in the WAGASCI detector, and the
369 reconstructed vertex is required to be inside a defined fiducial volume, $80 \times 80 \times 32 \text{ cm}^3$
370 region at the center of the detector, to reduce contamination from external backgrounds.
371 Second, at least one charged particle is required to reach to INGRID standard module
372 or Side-MRD modules, and it makes more than two hits in these sub-detectors. With the
373 event selection, expected numbers of the neutrino-candidate events during the beam period
374 are summarized in Table 1. Using the data, we will test the detector performance with
375 $\sim 3\%$ statistical uncertainties.

376 5 Detector performance

377 5.1 Wagasci module

378 To demonstrate the performance of the Wagasci module and also to study the neutrino
379 interaction, the first Wagasci module was installed at the on-axis position, in front of
380 the T2K INGRID horizontal center module in 2016. The INGRID module is made of iron
381 plates and segmented plastic scintillator bars. It's cross sectional size viewed from the beam
382 direction is $1 \text{ m} \times 1 \text{ m}$. The charged current interactions in the Wagasci module are selected
383 by requiring a muon track candidate in the INGRIRD modules. Here, we describe the
384 performance of the Wagasci module evaluated at this T2K on-axis measurement. Figure 20
385 shows the light yeild of channels for muons produced by the interaction of neutrinos in the
386 hall wall. The light yield is sufficiently hgh to get good hit efficieincy. A track search
387 algorithm based on the cellular automaton has been developed using the software tools by
388 the T2K INGRID. The tracking efficiency in 2-dimentional projected plane was evalualted
389 by comparing the reconstructed track in the Wagasci module and the INGRID module and
390 shown in Fig.21. Note that that the tracking efficinency for high angle ($> 70 \text{ deg}$) is not
391 evaluated because of the acceptance of the INGRID module, not because of the limitation
392 of the Wagasci module.

393 5.2 Baby MIND

394 The Baby MIND construction was completed in June 2017, and it was then tested in
395 June and July 2017 at the Proton Synchrotron experimental hall at CERN with a mixed
396 particle beam comprising mostly muons whose momenta could be selected between 0.5 and
397 5 GeV/c. An event display from the summer 2017 tests is shown in Figure 24.

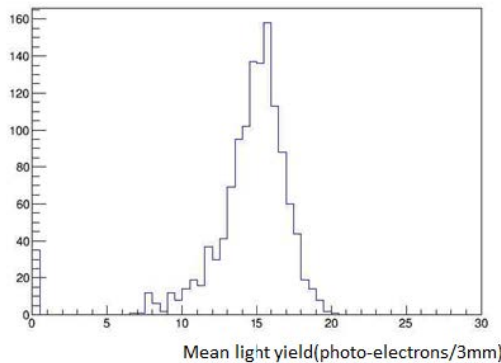


Figure 20: Light yield of channels for muons produced by the interaction of neutrinos in the hall wall.

398 All counters were measured at INR Moscow with a cosmic ray setup using the same
 399 type S12571-025C MPPCs and CAEN DT5742 digitizer [?]. The average light yield (sum
 400 from both ends) was measured to be 37.5 photo-electrons (p.e.) per minimum ionizing
 401 particle (MIP) and 65 p.e./MIP for vertical and horizontal counters, respectively. After
 402 shipment to CERN, all counters were tested once more individually with an LED test setup
 403 [?]. 0.1% of counters failed the LED tests and were therefore not used during the assembly
 404 of modules.

405 **5.3 Side muon range detector**

406 **6 MC studies**

407 **6.1 Detector simulation**

408 Expected number of neutrino events in the WAGASCI detector is evaluated with Monte
 409 Carlo simulations. Neutrino beam flux at the detector location is simulated by T2K neu-
 410 trino flux generator, JNUBEAM, neutrino interactions with target materials are simu-
 411 lated by a neutrino interaction simulator, NEUT, detector responses are simulated using
 412 GEANT4-based simulation. The neutrino flux at the detector location, 1.5 degrees away
 413 from the J-PARC neutrino beam axis, is shown in Figure 3, and its mean neutrino energy
 414 is around 0.68 GeV.

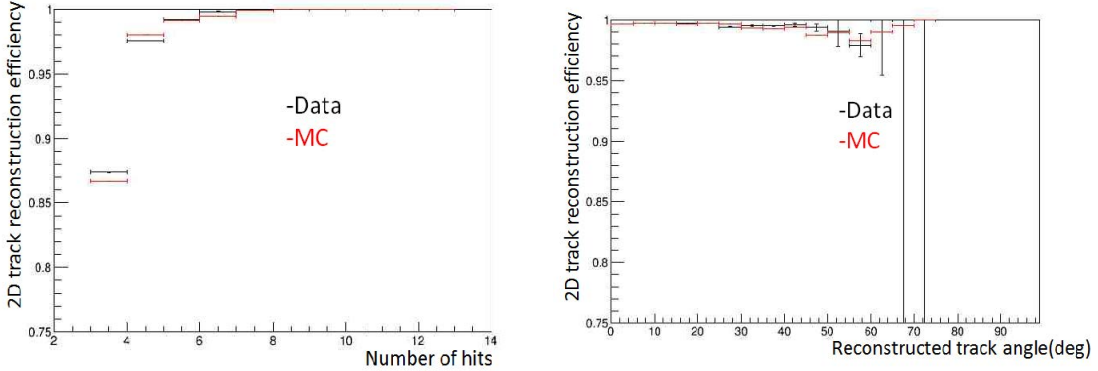


Figure 21: 2D track reconstruction efficiency as a function of number of hits (left) and track angle (right). Here the track angle is the one reconstructed by the INGRID module.

415 6.1.1 Detector geometry

416 The detector geometry in the GEANT4-based simulation is slightly different from the
 417 actual detector as shown in Fig. 26. The active neutrino target region consists of four
 418 WAGASCI modules, and each WAGASCI detector has the dimension with $100\text{ cm} \times 100$
 419 cm in the x and y directions and 50 cm along the beam direction. An event display of a
 420 MC event in the WAGASCI detectors is shown in Figure ???. Two Side-MRD modules is
 421 installed at both sides of the WAGASCI modules, and each Side-MRD module consists of
 422 ten iron plates whose dimension is $3\text{ cm (thickness)} \times 180\text{ cm (height)} \times 320\text{ cm (width)}$.
 423 The distance between the Side-MRD modules and WAGASCI modules is 60 cm. The
 424 downstream-MRD equivalent to the Baby-MIND is installed at the downstream of the
 425 WAGASCI modules. The downstream-MRD consists of ten iron plates whose dimension is
 426 $3\text{ cm (thickness)} \times 180\text{ cm (height)} \times 320\text{ cm (width)}$ and another ten iron plates whose
 427 dimension is $6\text{ cm (thickness)} \times 180\text{ cm (height)} \times 320\text{ cm (width)}$. The distance between
 428 the downstream-MRD modules and WAGASCI modules is 60 cm.

429 In order to estimate backgrounds from neutrino interactions in the wall and floor of the
 430 experimental hall, the geometry of the experimental hall is implemented in the GEANT4-
 431 based detector simulation.

432 6.1.2 Response of detector components

433 The energy deposit inside the scintillator is converted into the number of photons. The
 434 effects of collection and attenuation of the light in the scintillator and the WLS fiber are
 435 simulated, and the MPPC response is also taken into account. The light yield is smeared
 436 according to statistical fluctuations and electrical noise.

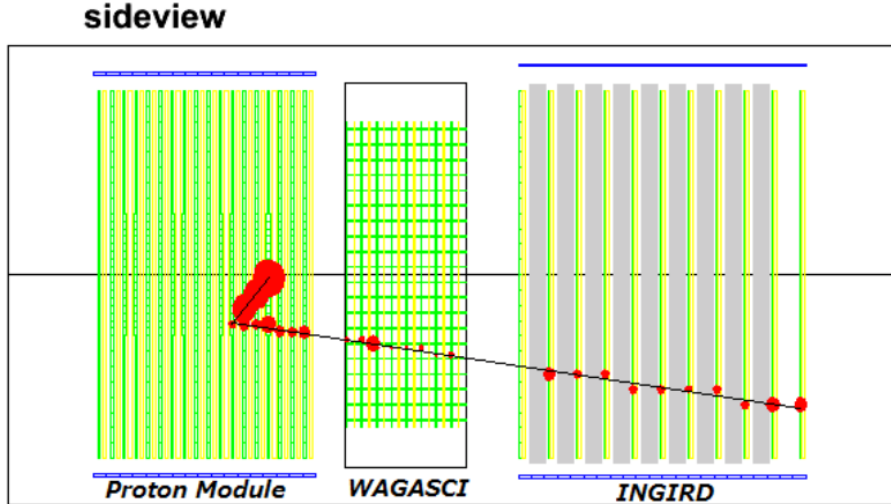


Figure 22: J-PARC T59 event display of a neutrino event in the GENAT4-based detector simulation.

437 6.2 Track reconstruction

438 To select neutrino interaction from the hit patterns, a track reconstruction algorithm is
 439 developed. The flow of the track reconstruction is as follows.

- 440 1. Two-dimensional track reconstruction in each sub-detectors
- 441 2. Track matching among the sub-detectors
- 442 3. Three -dimensional track reconstruction

443 Add explanation about two-dim reco, track matching and three-dim reco here.

444 6.3 Event selection

445 First, the events with the track which starts in 5 cm from the wall of the WAGASCI module
 446 are rejected to remove the background from the outside.

447 Second, to reject backgrounds from NC and neutral particles, the longest tracks are
 448 required to penetrate more than one (five) iron plates in Side-MRD modules (Baby-MIND).

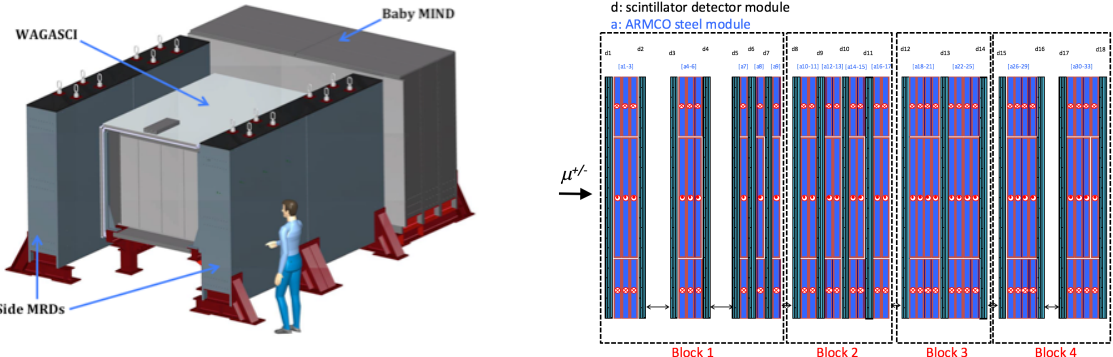


Figure 23: Left) WAGASCI modules: flanked by 2 side muon range detectors (sMRD) and one downstream muon detector (Baby MIND). Right) side view layout of the Baby MIND during beam tests at CERN.

449 Then, in order to measure muon momentum, the longest tracks are required to stop in
 450 MRDs (Side-MRD modules and Baby-MIND) or penetrate all iron plates.

451 Table 1 and 2 show numbers of the selected events after each event election in neutrino-
 452 mode and antineutrino-mode respectively. As for the neutrino-mode, 2.12×10^4 CC events
 453 are expected with 1×10^{21} POT, and the purity is 81.3 %. The main background for
 454 the neutrino-mode is the neutrino interactions in the scintillators inside the WAGASCI
 455 detector. As for the antineutrino-mode, 0.83×10^4 CC events are expected with $1 \times$
 456 10^{21} POT, and the purity is 62.0 %. The main background for the antineutrino-mode
 457 is the wrong sign contamination from ν_μ events and the antineutrino interactions in the
 458 scintillators inside the WAGASCI detector.

Table 1: Expected number of the neutrino-candidate events in two WAGASCI modules after the event selections with 1×10^{21} POT in neutrino-mode.

Cut	CC	NC	Scinti Bkg.	Total
Reconstructed	36186.4	1399.4	9396.5	46982.3
FV	30301.5	1176.8	7869.6	39347.8
Pene. iron	22528.5	474.6	5750.8	28753.9
Stop/Penetrate MRDs	16956.3	427.9	4346.1	21730.3
after all cuts	78.0 %	2.0 %	20.0 %	100 %

459 Figure 27 and 28 show the reconstructed angles of the longest tracks in the selected
 460 events in the neutrino-mode and the anti-neutrino mode respectively.

461 Figure 29 and 30 show the iron plane numbers corresponding to the end points of the
 462 longest tracks in the selected events.

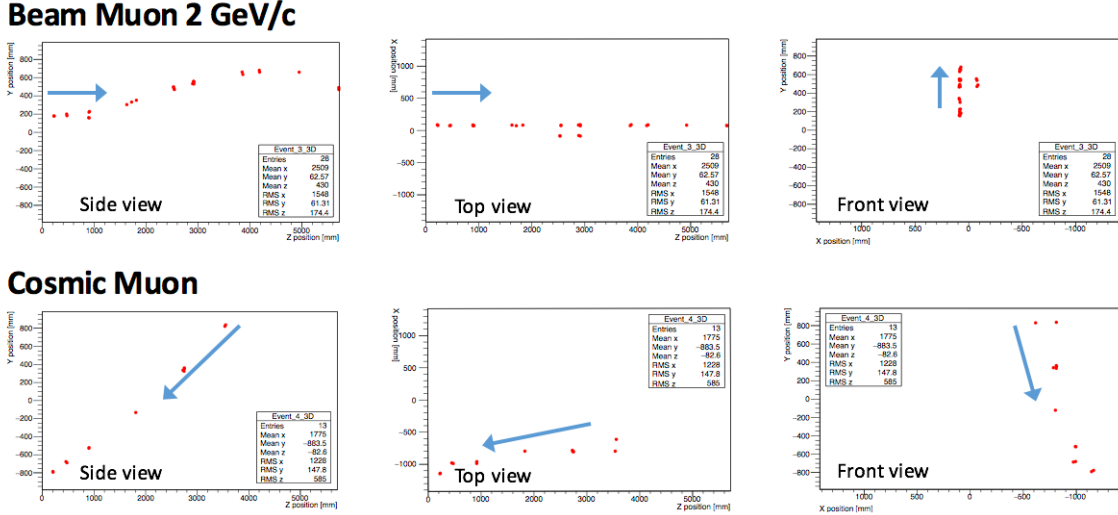


Figure 24: Comparison of a beam muon and cosmic muon in the three different geometrical projections of the detector. The beam impinges on the detector from the left. The arrows indicate the direction of travel of these muons. The direction of the cosmic muon is inferred from timing information.

463 6.4 Cross section measurements on water

464 In the water target events, the background from interaction with scintillators has to be
 465 subtracted by using the measurement of the hydrocarbon target.

466 **6.4.1 Charged current cross section measurement**

467 7 Standalone WAGASCI-module performances

468 In the previous sections, the WAGASCI detector was studied using the Muon Range Detectors.
 469 In this section, the standalone abilities of WAGASCI module are presented. Using
 470 the WAGASCI configuration presented in Section 6, we have evaluated that only 7% of
 471 the muons will be stopped in one of the WAGASCI modules. THowerver, this proportion
 472 increases to 53% for pions and 73% for protons produced by neutrino interactions at 1.5°
 473 off-axis. Figure 31 shows the momentum distribution of these daughter particles as well as
 474 for the sub-sample stopped in one of the WAGASCI modules. Therefore, the study of the
 475 standalone abilities of the WAGASCI module in this section are dominantly motivated by:

- 476 • the accurate measurement of the neutrino interaction final states. Though most of the
 477 muons will be reconstructed and identified in the MRDs, the hadronic particles will
 478 predominantly stops in one WAGASCI module. One has therefore to rely exclusively

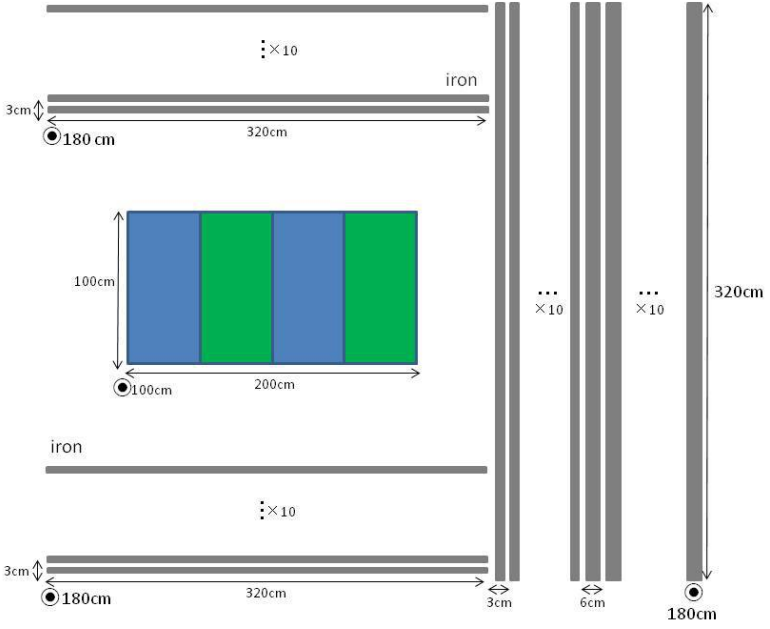


Figure 25: Geometry of the detectors in the Monte Carlo simulation.

479 on the WAGASCI module information alone to reconstruct, identify and measure the
 480 momentum of pions or protons.

- 481 • the coverage of the MRDs is not 4π . Using the WAGASCI module information can
 482 therefore help to constraint the particles that exits the WAGASCI module but do
 483 not geometrically enters any MRD.
- 484 • the particle identification of low momenta muons $p_\mu < 300 \text{ MeV}/c$ that will leave only
 485 few hits in the MRD. Using the WAGASCI module information will clearly enhance
 486 the particle identification.

487 This study is based on an original study done for the ND280 upgrade target, with some
 488 modifications. Though the cell size is similar to the WAGASCI configuration presented
 489 in Section 6, the external dimensions are different ($186.4 \times 60 \times 130 \text{ cm}^3$). Whenever the
 490 results are presented with this external size and this parameter is likely to impact the
 491 result, it will be mentioned.

492 Note that in this section, a simplified reconstruction algorithm presented in Section 7.1 is
 493 used. The fiducial volume is chosen accordingly as the inner cube of the module which
 494 surfaces are distant of $4 \times$ scintillator space = 10 cm from the module external surfaces.

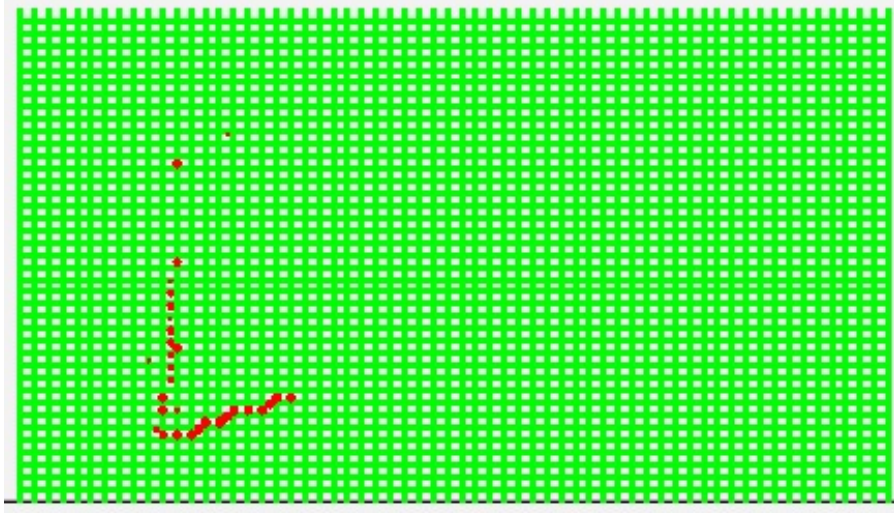


Figure 26: An event display of MC event in WAGASCI detectors. Green lines are scintillators and red circles are the hit channels.

495 The neutrino interactions are simulated using NEUT v5.3.2. The NEUT input neutrino
 496 flux is estimated using JnuBeam v13a and assuming the detector to be located at 1.5°
 497 off-axis, as in Section 6. Note that the event reconstruction efficiency as a function of true
 498 neutrino energy might be changed at 1.5° , due for example to different Q^2 distributions. For
 499 this reason, one has to note that the reconstruction results might slightly be changed from
 500 2.5° and 1.5° . To avoid a similar change on the particle-only reconstruction efficiencies,
 501 they will be presented as a function of variables that completely characterize the particle
 502 kinematic state, *i.e.* its momentum and angle. Figure 32 shows the vertices distributions
 503 of the daughter particles of neutrinos interacting one standard WAGASCI water-module.
 504 In this section, we will show the detector reconstruction and particle identification in this

Table 2: Expected number of the antineutrino-candidate events in two WAGASCI modules after the event selections with 1×10^{21} POT in antineutrino-mode.

Cut	CC	NC	Scinti Bkg.	Wrong sign bkg	Total
Reconstructed	12999.3	214.5	4468.8	4661.6	22344.2
FV	10915.7	178.6	3746.9	3893.1	18734.2
Pene. iron	8344.6	61.6	2881.8	3121.1	14409.1
Stop/Penetrate MRDs	6663.0	57.0	2240.6	2242.4	11202.9
after all cuts	59.5 %	0.5 %	20.0 %	20.0 %	100 %

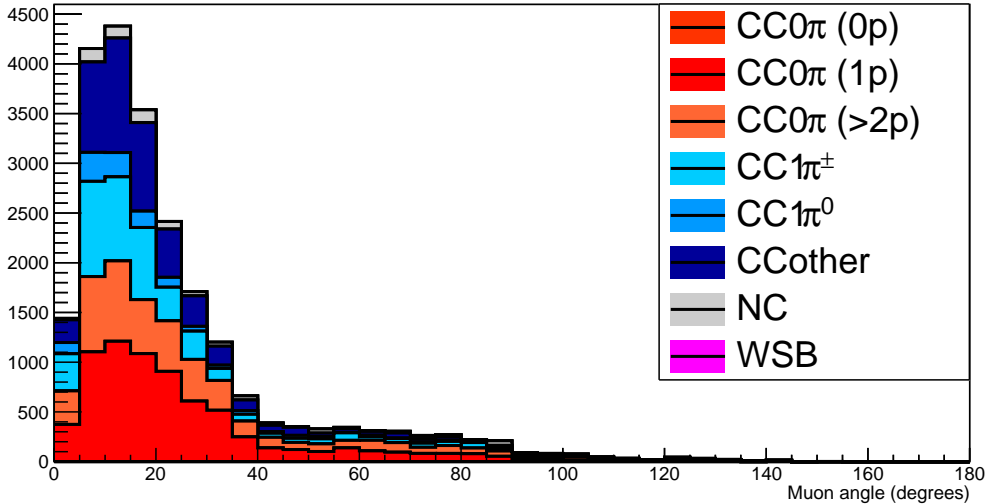


Figure 27: The reconstructed angles of the longest tracks in the selected events in the neutrino-mode.

phase space, both for leptonic and hadronic particles. We will finally show an empty WAGASCI module can highly enhance the ability to constrain the neutrino interaction final state which is critical to reduce the corresponding uncertainties.

7.1 Reconstruction algorithm

7.1.1 Description

For this section, an ideal “simulated” reconstruction is developed. A particle is reconstructed if:

1. The particle is charged.
2. Lets at least one hit (energy deposit > 2.5 photo-electron) in a scintillator.
3. The particle enters one TPC and let one hit in the tracker.

Or

- The particle should be long enough to be reconstructed by the detector in at least 2 out of 3 views (XZ, YZ, XY). The length criterion requires the particle

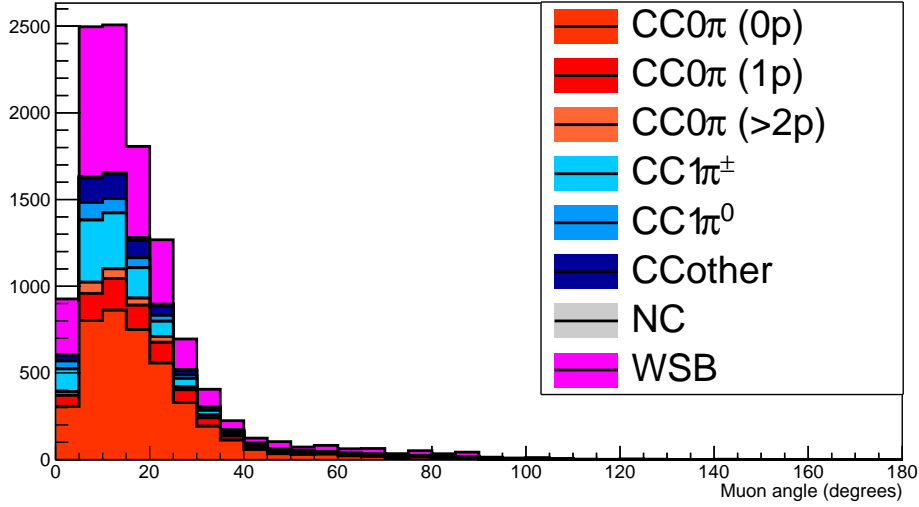


Figure 28: The reconstructed angles of the longest tracks in the selected events in the antineutrino-mode.

to let at least 4 hits in the detector. In the “less favourable case” of pure longitudinal or transverse going tracks, it represents a the track length of $L_{track} \geq 4 \times \text{scintillator space} = 10.0 \text{ cm}$.

- In the views where particles pass the length criterion, the particle shall not be superimposed with longer tracks in at least two views. The superposition criterion is estimated with the distance inter-tracks (DIT) which corresponds to the orthogonal distance between two tracks at the ending point of the shortest one (see Figure 33). For a track 1, the superposition criterion is tested with every longer tracks that starts at the same vertex. Let \vec{p}_1 the vector of track 1, and \vec{p}_1^a its projections in the XZ, YZ and XY planes respectively for $i=1,2,3$. Note that these are projections in a 2D planes and not on a direction vector. In this case, the relative angle between the track 1 and a longer track 2 (of vector \vec{p}_2) in a view a is given by:

$$\cos \theta = \frac{\vec{p}_1^a \cdot \vec{p}_2^a}{\|\vec{p}_1^a\| \|\vec{p}_2^a\|} \quad (1)$$

and the distance inter track is given by:

$$\text{DIT} = \|\vec{p}_1^a\| \sin \theta \quad (2)$$

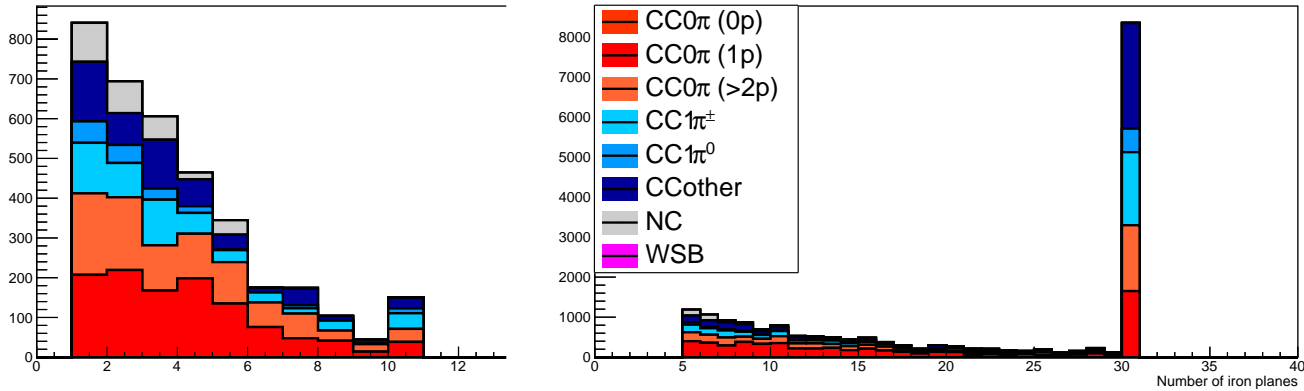


Figure 29: Iron plane numbers in Side-MRD (left) and Baby-MIND (right) corresponding to the end points of the longest tracks in the selected events in the neutrino-mode.

534 The DIT should be higher than $4 \times$ scintillator width for the track 1 to be not
 535 superimposed with the track 2 in the view a, which also corresponds to 10.0 cm
 536 in the nominal configuration.

537 **7.1.2 Performances**

538 The particle-only reconstruction efficiencies and the reconstruction threshold in momenta
 539 are shown in Table 3. This threshold is defined as the maximal momentum for which the
 540 reconstruction efficiency is smaller than 30%. The thresholds in muon and pion momenta
 541 are 150 MeV/c. Most of the muons are above this threshold (see Figure 32) which leads
 542 to a 79% reconstruction efficiency.

	μ	π	p
Reconstruction Efficiency Momentum threshold	79%	52%	26%
	150 MeV/c	150 MeV/c	550 MeV/c

Table 3: Reconstruction efficiency and momentum threshold for muons, pions and protons. The threshold is defined as the maximal momentum for which particles have a reconstruction efficiency smaller than 30%.

543 The lower pion and proton efficiencies (respectively 52% and 26%) are due to lower
 544 efficiencies for similar momenta than muons, coming from strong interactions as shown
 545 on Figures 34. Efficiencies of each particle type tend to decrease in the backward region

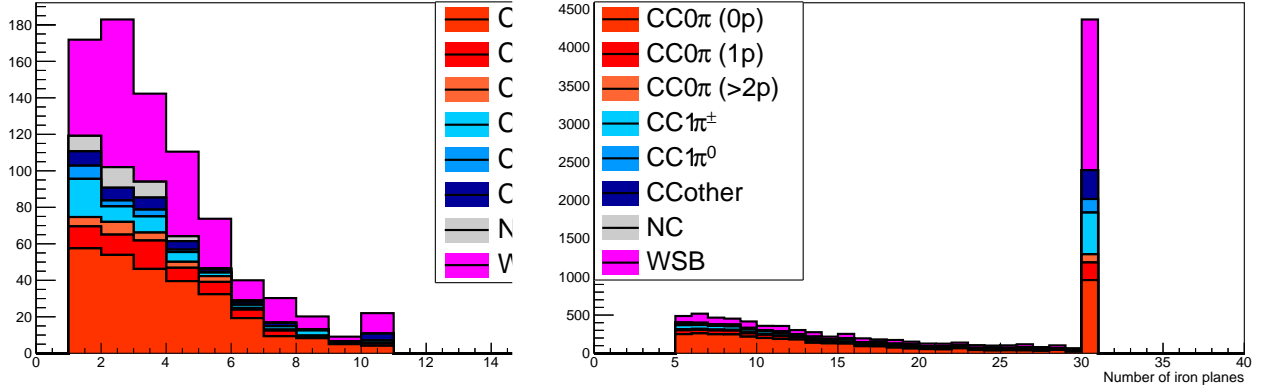


Figure 30: Iron plane numbers in Side-MRD (left) and Baby-MIND (right) corresponding to the end points of the longest tracks in the selected events in the antineutrino-mode.

due to particle lower momenta. However, for a fixed momentum value, the reconstruction efficiency is almost uniform which confirms the ability of the WAGASCI detector to reconstruct high angle tracks.

The reconstruction is thereafter tested on neutrino events. Table 4 summarizes the number of reconstructed events and efficiencies for each interaction type. As expected from the high muon reconstruction efficiency, the charged current interactions have reconstruction efficiencies $\geq 85\%$.

	CC0 π	CC1 π	CCOthers	NC	All
Reconstruction efficiency	85%	87%	91%	22%	68%

Table 4: Number of true interactions reconstructed. The purity and reconstruction efficiency of each true interaction is also shown.

The reconstruction efficiencies as a function of the neutrino energy and muon kinematics are respectively shown on Figure 35 and 36.

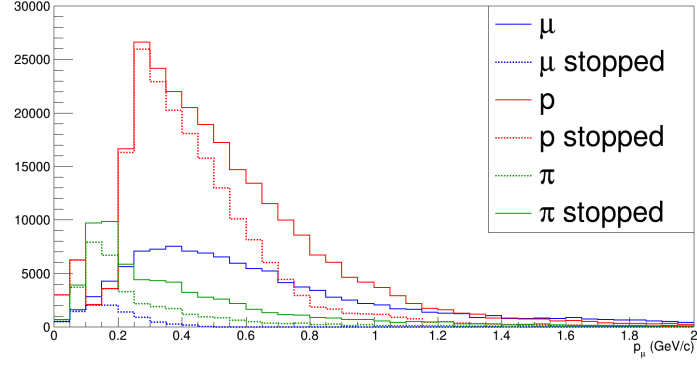


Figure 31: Momentum distribution of true particles in WAGASCI (plain) and corresponding distributions only for particles stopping into the WAGASCI module (dashed).

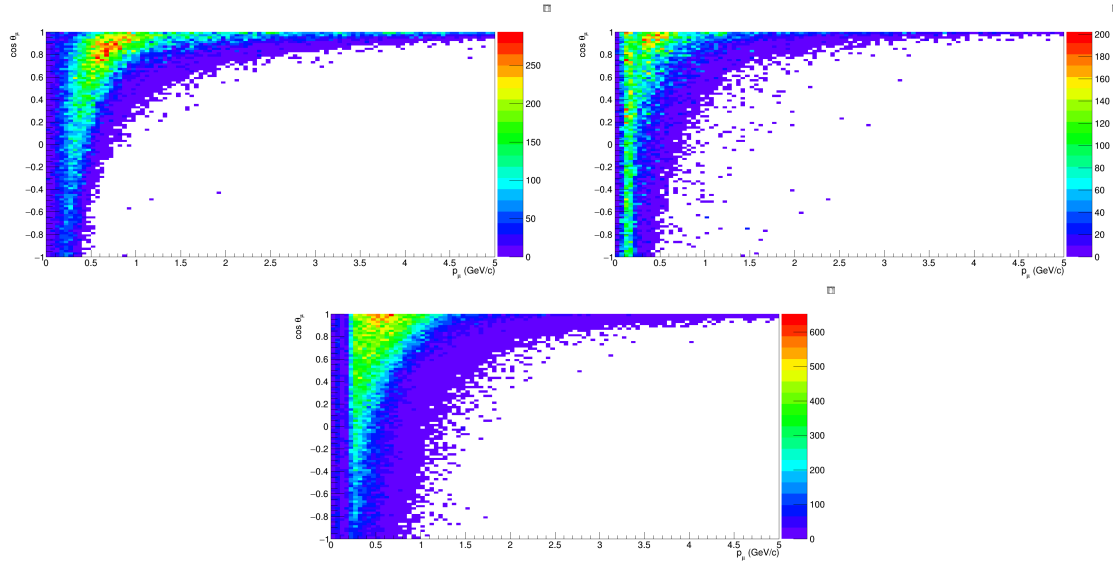


Figure 32: True number of muons (left), charged pions (right) and protons (bottom) in the two WAGASCI water-module as a function of the particles momenta and angles at 1.5° .

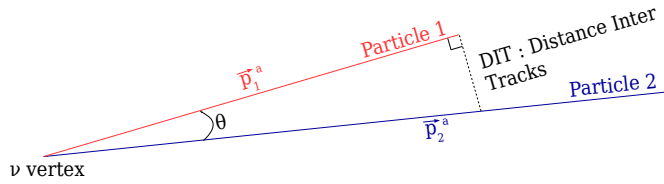


Figure 33: Definition of the distance inter tracks.

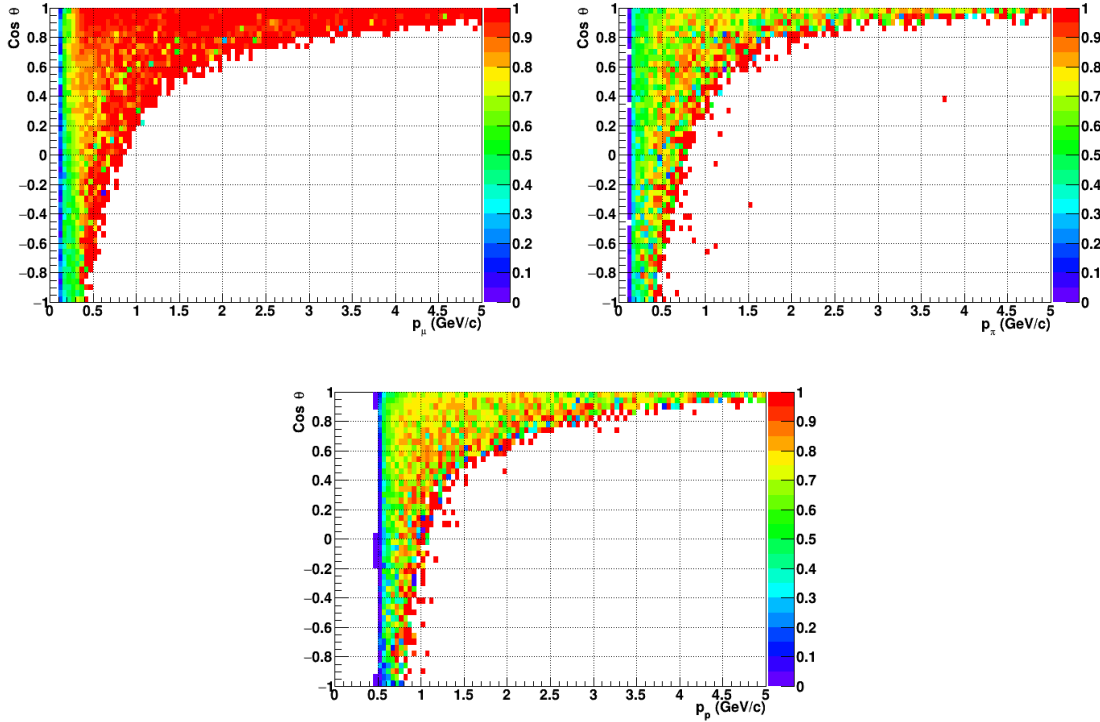


Figure 34: Reconstruction efficiency of muons (left), charged pions (right) and protons (bottom) in the WAGASCI water-module as a function of the particles momenta and angles.

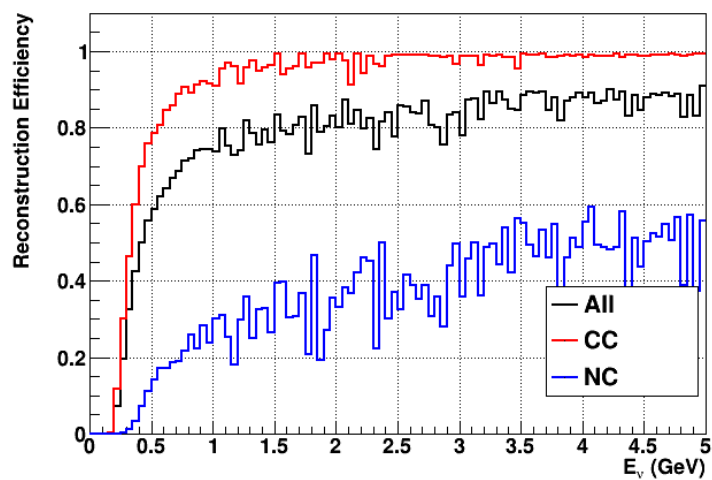


Figure 35: Reconstruction efficiency of all neutrino (black), CC (red) and NC (blue) interactions in the WAGASCI water-module as a function of the neutrino energy.

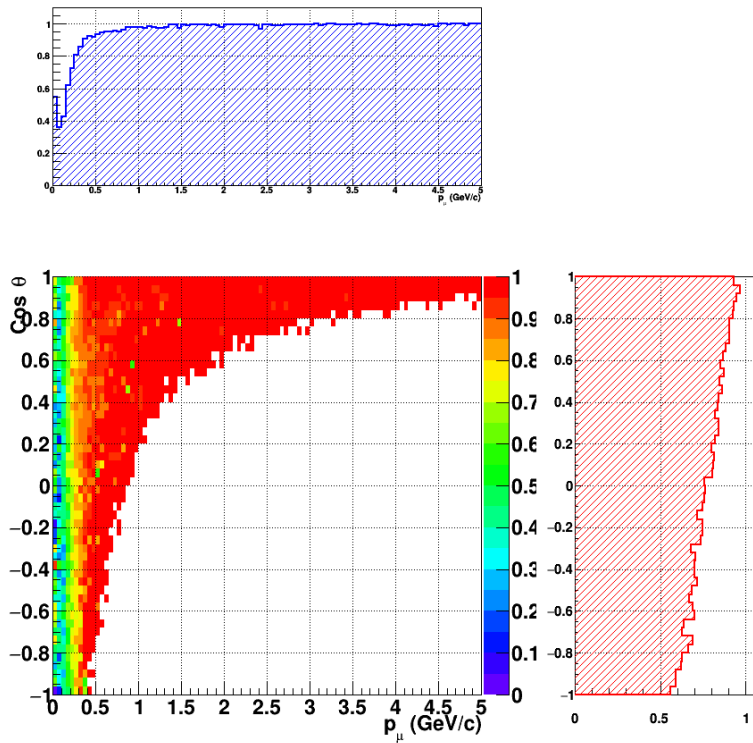


Figure 36: Reconstruction efficiency of CC interactions in the WAGASCI water-module as a function of the muon kinematic variables (momentum and angle).

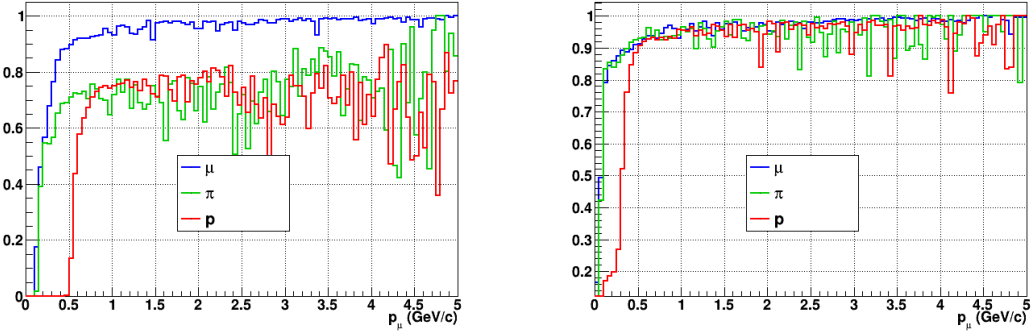


Figure 37: Reconstruction efficiency for muons, pions and protons in the water-in (left) and water-out (right) modules.

555 Note that a Particle Identification Algorithm has been also developed. It is based on
 556 the charge deposition of the particles in the scintillator, of the detection of a decay-electron.
 557 However, this information highly depends on the number of scintillator hit by a particle,
 558 which creates an important difference between a real WAGASCI module and the one used
 559 for the ND280-upgrade simulation. For this reason, the corresponding results will not be
 560 detailed here, but can be found in [?].

561 7.2 Background subtraction: the water-out module

562 In the nominal configuration, 20% of the neutrino interactions occurs on scintillators
 563 (C_8H_8). This background should be removed in order to measure the neutrino interac-
 564 tion on the same target as Super-K, which suppress the differences in cross-section models.
 565 For this purpose, we propose to use a water-out module, where the water is replaced by
 566 air. The detector is therefore fully active and has a 3 mm spatial resolution (scintillator
 567 thickness) which create an ideal detector to reconstruct and identify hadrons, and study
 568 np-nh interactions. The counter-part is the difference in particle energy deposition between
 569 the water and this water-out module that will need to be corrected for. In this section,
 570 we present the capabilities of such a module, and the impact it can have on cross-section
 571 measurements for the neutrino community in general and T2K in particular.
 572 The same reconstruction and selection as the water-in module is applied. Figure 37 shows
 573 the comparison between the water-in and the water-out reconstruction efficiencies for muon,
 574 pions and protons. 90% of the muons and 87% of the pions are reconstructed, while 70%
 575 of the protons are even reconstructed. It allows to lower down the proton threshold to
 576 250 MeV/c (see Table 5).

577 As a consequence of tracking even low momenta particle, the reconstruction efficiency
 578 is uniform and almost maximal on the entire $\cos \theta_\mu$ phase space, as shown on Figure 38.

	μ	π	p
Reconstruction Efficiency Momentum threshold	90% 50 MeV/c	87% 50 MeV/c	70% 250 MeV/c

Table 5: Reconstruction efficiency, proportions of μ -like and non μ -like and momentum threshold for muons, pions and protons in the empty module. The threshold is defined as the maximal momentum for which particles have a reconstruction efficiency smaller than 20%.

579 Since the fiducial mass represents 0.25 tons, the total number of events is divided by a
 580 factor of 3 compared to the water-in module. The water-out module offers interesting
 581 possibilities to study np-nh interaction since 70% of the protons are reconstructed. In the
 582 future, a possible separation as a function of the number of proton track will be studied.
 583 Moreover, we are currently pursuing the use of single and double transverse variables (cite
 584 Xianguo) to open new possibilities for separating np-nh from Final State Interactions, or
 585 for isolating the interactions on hydrogen from interactions on carbon in this module.

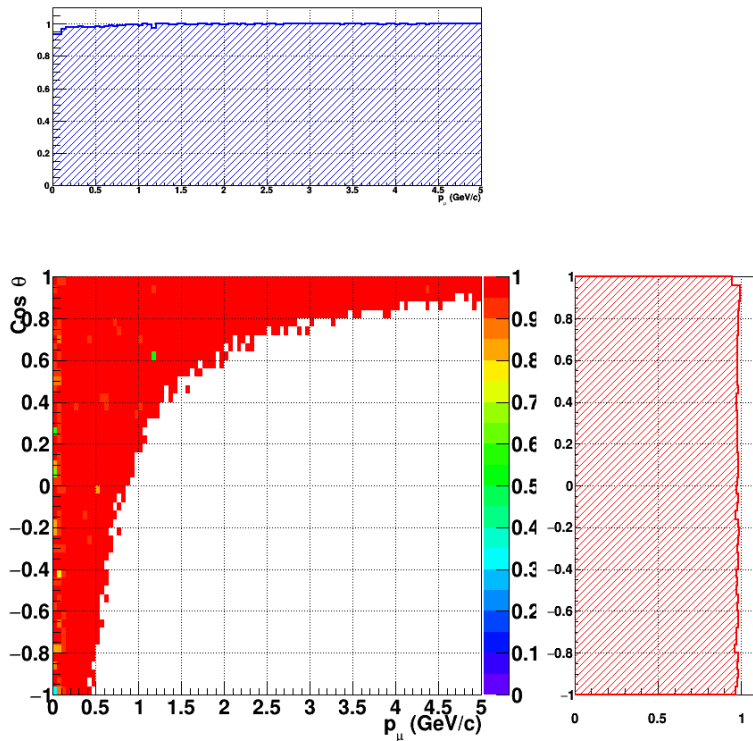


Figure 38: Reconstruction efficiency of CC interactions in the WAGASCI empty module as a function of the muon kinematic variables (momentum and angle).

586 **8 Schedule**

587 We would like to start a physics data taking from T2K beam time after the summer
588 shutdown in 2018. By then, commissioning and tests of the detectors will be completed
589 in J-PARC T59. The experiment can run parasitically with T2K, therefore we request no
590 dedicated beam time nor beam condition as discussed in the following section.

591 Once the approved POT is accumulated, the WAGASCI modules will be removed
592 from the experimental site, but we would like to keep the Baby-MIND and the Side-MRD
593 modules on the B2 floor of the NM pit as common platforms of future neutrino experiments
594 using the T2K neutrino beam.

595 **9 Requests**

596 **9.1 Neutrino beam**

597 The experiment can run parasitically with T2K, therefore we request no dedicated beam
598 time nor beam condition. As data taking periods, we request the ‘nominal’ T2K one-year
599 operation both for the neutrino beam and the antineutrino beam. The T2K has been
600 requesting 0.9×10^{21} POT/year and actually accumulating about 0.7×10^{21} POT/year in
601 recent years. For each year, starting from the Autumn, T2K is running predominantly in
602 the neutrino mode or in the antineutrino mode. Our request is to have one-year neutrino-
603 mode data and another one-year antineutrino mode data assuming that the POT for the
604 fast extraction in each year is more than 0.5×10^{21} POT.

605 **9.2 Equipment request including power line**

606 We request the followings in terms of equipment on the B2 floor:

- 607 • Site for the WAGASCI modules, Side-MRD modules and BabyMIND and their elec-
608 tronics system on the B2 floor of the near detector hall (Fig. 2).
- 609 • Anchor points (holes) on the B2 floor to secure the WAGASCI modules, Side-MRD
610 module and Baby-MIND (Fig. ??)
- 611 • Power line for the magnets in Baby-MIND: 400 V tri-phase 48-to-62 Hz, capable of
612 delivering 12 kW.
- 613 • Electricity for electronics and water circulation system, 3 kW, standard Japanese
614 electrical sockets.
 - 615 1. Online PCs: 2.1 kW
 - 616 2. Electronics: 0.7 kW
 - 617 3. Water sensors: ?

- 618 • Air conditioner for cooling heat generation at Baby-MIND magnets, online PCs and
619 electronics
- 620 • Beam timing signal and spill information
- 621 • Network connection

622 **9.2.1 Baby MIND Equipment request including power line**

623 We request the following in terms of equipment on the B2 floor:

- 624 • Site for the Baby MIND detector and its electronics systems on the B2 floor of the
625 near detector hall.
- 626 • Anchor points (holes) on the B2 floor to secure the 9 support frames, of order 4 holes
627 per frame, detailed floor plans to be communicated in a separate document.
- 628 • Power line for the magnet: 400 V tri-phase 48-to-62 Hz, capable of delivering 12
629 kW. We have a wish for the magnet power line to be installed and available to us by
630 beginning of March 2018.
- 631 • Electricity for electronics, 1 kW, standard Japanese electrical sockets.
- 632 • Beam timing signal and spill information
- 633 • Network connection

634 The infrastructure for much of the above exists already, and will be shared in part with
635 the WAGASCI experiment. Exceptions are the power line for the magnet and holes in the
636 B2 floor to anchor the detector support structures.

637 **10 Conclusion**